

## Light scattering study of boron nitride microcrystals

R. J. Nemanich

*Xerox Palo Alto Research Center, Palo Alto, California 94304*

S. A. Solin

*Department of Physics, Michigan State University, East Lansing, Michigan 48864*

Richard M. Martin

*Xerox Palo Alto Research Center, Palo Alto, California 94304*

(Received 10 November 1980)

Raman scattering and x-ray diffraction measurements are used to correlate finite-size effects on the Raman spectra of nonpolar vibrational modes in BN. The BN microcrystalline samples used exhibited domain sizes varying from 4.4 to 78.5 nm in the plane and 1.5 and 47.5 nm perpendicular to the planes. The Raman measurements indicated that the high-frequency  $E_{2g}$  mode shifted to higher frequency and broadened as the crystallite size decreased. A formulation of the Raman cross section for scattering from nonpolar microcrystals is presented. The development includes evaluation of the susceptibility correlation function over a limited spatial extent. The results indicate that spectral changes are related to the phonon dispersion, and the wave-vector uncertainty is accounted for. The formulation is applied to describe the BN light scattering results, and good agreement was obtained to describe the observed shift in frequency.

### I. INTRODUCTION

To date there have been a number of experimental and theoretical studies of finite-size effects on the polar vibrational excitations of small ionic crystals. The status of this area of research was reviewed thoroughly in 1970 by Ruppin and Englman<sup>1</sup> who have pointed out several general properties of ionic crystals. They noted that the Raman spectra of a thin slab of ionic crystal should exhibit wave-vector-dependent surface modes (polaritons) as well as bulk transverse and longitudinal phonons. Similar effects were predicted for oriented particles of different shapes.<sup>2</sup> These predictions have been experimentally supported for several materials.<sup>3-5</sup> Implicit in the review of Ruppin and Englman is the theoretical approximation that experimental measurements of finite-size effects could be carried out on samples of noninteracting, identically oriented crystallites. That approximation is seldom valid; real samples such as powders will in general contain randomly oriented interacting crystallites with a distribution of sizes and shapes. Martin and Genzel<sup>6</sup> have considered the effect of powder density on the Raman scattering from small ionic crystals. They showed that the transverse and longitudinal phonon frequencies are affected by the local electric field which depends on the surface polarization and therefore on the powder density.

The traditional theoretical and experimental emphasis on polar modes in ionic crystals is not surprising since such modes are expected to

exhibit the most dramatic effects with decreasing crystal size. On the other hand, more subtle yet equally interesting size effects, which are best explored by examining nonpolar modes, have received some recent interest. A theoretical development has considered the scattering due to the surface atoms of finite-sized crystals.<sup>7</sup> In addition two nonpolar materials in which effects have been observed in the Raman spectra due to finite-size crystals are graphite<sup>8-12</sup> and Si.<sup>13,14</sup> In order to understand the results for Si, calculations of the long-wavelength modes of a thin slab were carried out.<sup>15</sup> For graphite, wave-vector selection-rule breakdown was proposed to account for the observed effects in both the first- and second-order Raman scattering.<sup>8-11</sup> These results suggest that at sufficiently small crystallite size ( $\leq 30$  nm), the Raman scattering and ir absorption wave-vector selection rules which limit the wave vector of detectable phonons to the Brillouin-zone center break down. While the experimental observations have been accounted for by invoking selection-rule breakdown, it has, however, only casually been discussed and has not been the subject of any systematic experimental study. In addition one expects the lifetimes and frequencies of nonpolar phonons to exhibit measurable changes when the crystal size is  $\leq 30$  nm. The convolution of these changes with the selection-rule relaxation should significantly alter the optical properties, particularly the Raman spectra. Accordingly, we report in this paper a systematic study of the effect of crystallite size on the Raman spectra of the nonpolar intralayer

mode of hexagonal boron nitride.

While BN also exists in the zinc-blende and wurtzite structures,<sup>16</sup> this study will only be concerned with the hexagonal layer structure.<sup>17,18</sup> Hexagonal boron nitride, like graphite, is one of the prototypical lamellar materials primarily because its layers are indeed planar.<sup>17,18</sup> The layers exhibit the same hexagonal structure as in graphite except the atoms are alternating B and N. The planar stacking in BN is, however, somewhat different than in graphite. In BN the planes align such that the hexagons reside directly above one another, and the atoms immediately above or below in adjacent planes are of the opposite species. This stacking arrangement is to be contrasted with graphite, where half the atoms sit over a hexagon center in adjacent planes. A schematic diagram of the BN crystal structure is shown in Fig. 1.

An interesting property of BN is that it is possible to prepare microcrystalline powders for which the average crystallite has a typical basal plane dimension which can be varied from ~3 to 1000 nm.<sup>19</sup> Moreover, BN exhibits a very strong nonpolar intralayer Raman line at ~1370  $\text{cm}^{-1}$  (Ref. 20) which can be easily probed experimentally even with powder samples which show intense parasitic scattering at low-frequency shifts. Thus hexagonal BN microcrystals constitute a relatively ideal system with which to study the effects of crystal size on the Raman spectra of nonpolar vibrational excitations. Essential to such a study is the determination of crystallite size. We have accomplished this by

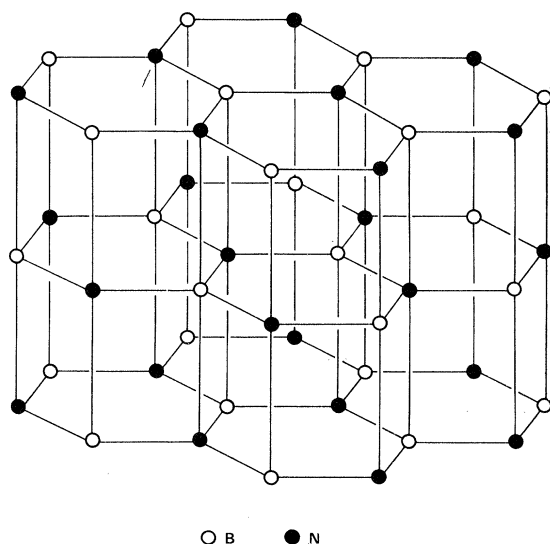


FIG. 1. The crystal structure of hexagonal BN.

using x-ray scattering measurements from the same samples from which the Raman spectra were obtained.

In order to understand the changes associated with reduced size we have carefully examined and analyzed the Raman spectra of large BN crystals. This spectrum was first observed by Geick *et al.*<sup>20</sup> who detected only one of the two group-theoretically predicted Raman-active modes, the intralayer mode. Subsequently the low-frequency rigid-layer shear mode was observed independently by two groups<sup>21,22</sup> and the pressure dependence was studied by Kuzuba *et al.*<sup>23</sup> However, as noted above, we will in this paper focus on the intralayer mode. The results presented here show that this mode shifts to higher frequency and broadens markedly with decreasing crystallite size. Moreover, we will develop a phenomenological model for the light scattering cross section of small crystals and employ that model to quantitatively account for the dependence of the intralayer mode of BN on crystallite size.

## II. EXPERIMENTAL

### A. Sample preparation and characterization

The samples of BN microcrystalline powders have been prepared following a method reported by Thomas *et al.*<sup>19,24,25</sup> In this procedure "turbostratic" BN is first prepared. It has been suggested that the "turbostratic form" consists of the hexagonal layers which, while oriented parallel to each consecutive layer, are randomly oriented with respect to axes in the plane.<sup>19</sup> The size of the crystalline domains can then be increased by heating the turbostratic material in a closed crucible.<sup>19</sup>

The first step of the process, preparation of turbostratic BN, was carried out by heating urea and orthoboric acid to 900°C under a flow of  $\text{NH}_3$ . The time of heating was varied from 2 to 6 hours. The oven configuration is shown in Fig. 2(a). The mixing of orthoboric acid and urea was carried out by grinding the reagent-grade powders by hand using a mortar and pestle. Typically, 20.0 g of urea were mixed with 10.3 g of orthoboric acid. The resultant powders exhibited a gritty texture, were slightly yellow, and would not dissolve readily in water.

To obtain powders with larger microcrystalline domains the turbostratic BN samples were heated in a closed graphite crucible to between 1400 and 1900°C using rf induction. Between 2 and 3 g of turbostratic BN were typically used. The heating arrangement is shown in Fig. 2(b). In some cases, a small amount (~0.01 g) of fully ordered BN was added to act as a seed. Again, the results of all

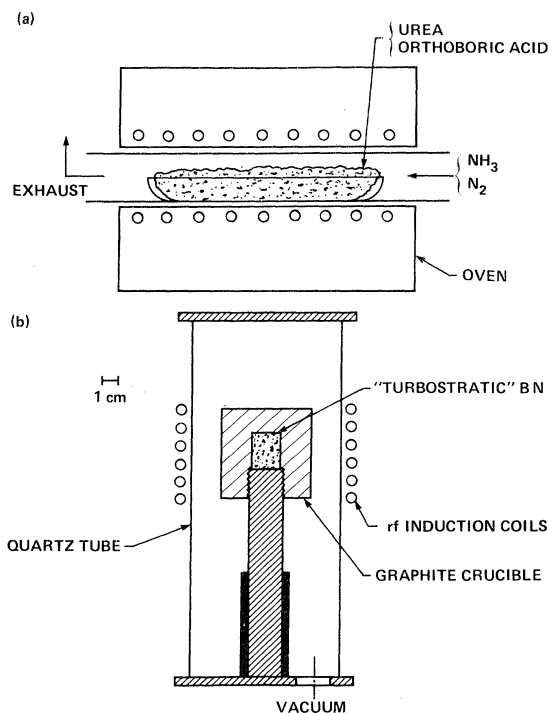


FIG. 2. (a) The oven configuration used to produce "turbostratic" BN and (b) the heating arrangement used to produce BN with larger crystalline domain sizes.

runs yielded a gritty slightly yellow powder. The material closest to the crucible walls was most yellowed, and this material was discarded. In addition to the prepared samples, two commercially prepared powders were studied, and a highly ordered sample prepared by compression annealing of pyrolytic BN (Ref. 26) was obtained from A. W. Moore of Union Carbide.

The x-ray diffraction and Raman studies were carried out on ~1-cm diam. pellets ~1 to 2 mm thick which were pressed from the powders. The powders were pressed in an evacuated holder, and no sintering agent was used. In order to characterize the samples and to determine the microcrystalline domain sizes, x-ray diffraction traces were obtained using chromium radiation. Several of the traces recorded are shown in Fig. 3. The samples labeled XBN-1 and XBN-2 were the commercially obtained reagent-grade powders which exhibited full ordering. All other samples displayed were prepared using the methods described above.

The x-ray diffractometer patterns obtained from these samples exhibited two broad peaks. The trace labeled XBN-9 in Fig. 3 is a pattern obtained from the turbostratic form and is consistent with that reported by Thomas *et al.*<sup>19</sup> The

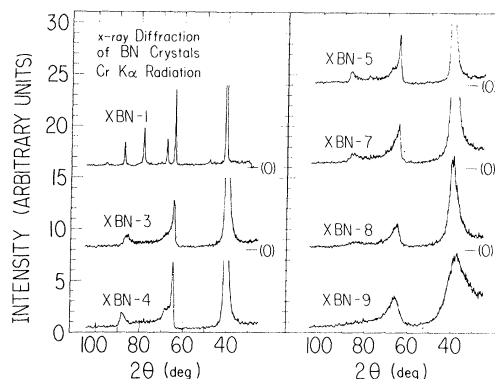


FIG. 3. The x-ray diffractometer traces of several of the BN powders.

microcrystalline domain sizes were obtained using the Scherrer formula.<sup>27</sup> This formula relates x-ray diffraction peak widths to microcrystalline domain sizes and is given by

$$L = k\lambda / (B^2 - B_i^2)^{1/2} \cos\theta. \quad (1)$$

Here  $B$  is the full width at half maximum (FWHM) of the respective peaks in the  $2\theta$  trace,  $\lambda$  is the x-ray wavelength, and  $B_i$  is the instrumental contribution. For  $L_a$ , the planar domain size,  $k=1.84$ , and for  $L_c$ , the domain extent perpendicular to the planes,  $k=0.9$ .

In order to obtain  $L_a$  the width of the (10) reflection which occurs at  $2\theta \approx 66^\circ$  is used, while for  $L_c$  the width of the (002) reflection which occurs at  $2\theta \approx 40^\circ$  is used. The results of  $L_c$  and  $L_a$  obtained using this method are shown in Table I. An interesting aspect of the measurements is that the  $L_c/L_a$  ratio is approximately constant for all the prepared samples, as indicated in Table I. While it is certain that there is a distribution of domain sizes in these powders, it is difficult to ascertain parameters to describe it. It seems clear that the values obtained describe the most probable domain sizes.

#### B. Raman measurements

The Raman scattering measurements were carried out in a backscattering geometry. About 100 mW of 514.5-nm Ar-ion laser radiation was incident on the sample at  $\sim 45^\circ$  from normal. The scattered light was collected using  $\sim F1$  optics at  $90^\circ$  from the incident light. The scattered light was dispersed with a Jarrell-Ash 1-m double monochromator equipped with holographic gratings. In the case of the highly oriented BN a triple monochromator system was used to obtain high-resolution low-frequency spectra. For the powdered samples a strong luminescence background was often observed. It was found that

TABLE I. The x-ray-determined average crystalline domain dimensions and the ratio of those dimensions.  $L_c$  is the range of order perpendicular to the planes, and  $L_a$  is the range of order in the planes.

Sample	$L_a$ (nm)	$L_c$ (nm)	$L_c/L_a$
XBN-1	$78.5 \pm 13.0$	$47.5 \pm 11.0$	$0.60 \pm 0.24$
XBN-2	$56.4 \pm 6.5$	$35.3 \pm 6.0$	$0.63 \pm 0.17$
XBN-3	$20.2 \pm 2.0$	$9.7 \pm 0.8$	$0.48 \pm 0.09$
XBN-4	$22.5 \pm 2.4$	$10.9 \pm 0.8$	$0.48 \pm 0.09$
XBN-5	$24.3 \pm 2.5$	$10.0 \pm 0.8$	$0.41 \pm 0.08$
XBN-6	$17.8 \pm 2.0$	$7.4 \pm 0.5$	$0.42 \pm 0.08$
XBN-7	$9.0 \pm 1.3$	$4.2 \pm 0.4$	$0.47 \pm 0.11$
XBN-8	$7.2 \pm 0.8$	$2.9 \pm 0.2$	$0.40 \pm 0.07$
XBN-9	$4.4 \pm 0.5$	$1.5 \pm 0.2$	$0.34 \pm 0.08$

laser illumination for several hours caused a marked decrease in the luminescence. Since BN has a band gap of  $> 5$  eV,<sup>28</sup> this luminescence arises from impurities and/or defects, and oxygen or carbon impurities may be likely candidates.

### III. RESULTS AND DISCUSSION

#### A. Large crystals

The largest crystalline domains studied were found in the oriented BN sample. Crystalline BN has  $D_{6h}^4$  space-group symmetry and the symmetry<sup>13</sup> transformations of the zone-center optic phonons are given by<sup>20</sup>

$$\Gamma = 2E_{2g} + 2B_{1g} + A_{2u} + E_{1u}. \quad (2)$$

Of these, the  $E_{2g}$  modes are Raman active, the  $A_{2u}$  and  $E_{1u}$  modes are ir active, and the  $B_{1g}$  modes are optically inactive. The Raman spectrum obtained from the highly oriented compression-annealed BN is shown in Fig. 4. The two modes clearly evident at 1366.2 and 51.8  $\text{cm}^{-1}$  are attributed to the  $E_{2g}$  symmetry vibrations. The large anisotropy of inter- and intraplanar bonding is reflected in the large difference in the frequencies of these modes. Both modes are due to in-plane atomic displacements, but the low-frequency mode is characterized by whole planes sliding against each other. This action has been termed a "rigid-layer shear mode." In contrast the high-frequency mode is due to B and N atoms moving against each other in a plane.<sup>20</sup> It is interesting to compare BN with graphite, which exhibits an identical space-group symmetry. In graphite the  $E_{2g}$  modes have been observed at 42 and 1581  $\text{cm}^{-1}$ .<sup>29</sup> Since the mode effective masses of BN and graphite are nearly identical, the slightly higher rigid-layer frequency of BN is indicative of slightly stronger interplanar bonding.

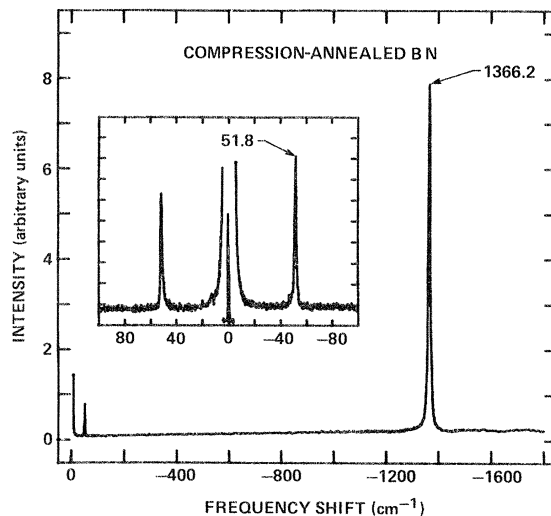


FIG. 4. The Raman spectrum of highly oriented compression-annealed BN. The two peaks are attributed to the  $E_{2g}$  symmetry vibrations. The inset shows the Stokes and anti-Stokes low-frequency spectrum taken with a higher resolution.

#### B. Microcrystalline BN

From the x-ray diffraction results it might be expected that microcrystalline domains will affect the light scattering spectrum. The high-frequency Raman spectra of the powder samples are shown in Fig. 5. We were not able to observe the low-frequency rigid-layer mode in any of the prepared samples due to strong elastic scattering and a broad luminescence background. The Raman spectra showed no new features, and from here on we will concentrate on the spectral changes of the 1366- $\text{cm}^{-1}$  line. There are two effects which are evident in Fig. 5. Clearly the peak broadens and shifts to higher frequency as the crystal domain size decreases. While the broadening may not be unexpected, we find it some-

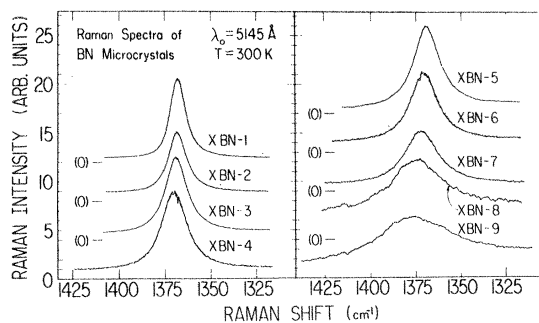


FIG. 5. The Stokes-shifted Raman spectra of the BN powders. The dependence of the high-frequency  $E_{2g}$  mode is shown.

what unusual that the mode shifts to higher frequency.

The results are quantified in Figs. 6 and 7. The peak shift  $\Delta$  and the full width at half maximum  $\Gamma_{1/2}$ , are plotted versus  $1/L_a$ . Here  $\Delta$  is the frequency shift of the peak from the value corresponding to the largest crystallite sample, XBN-1. In each case the data exhibits a linear dependence on  $1/L_a$  and the results of a least-squares fit are shown in Figs. 6 and 7.

### C. Analysis of domain-size dependence

In this subsection we will explore the relation of wave-vector selection conditions and crystal domain size. The BN system is well suited to this kind of analysis because the  $E_{2g}$  mode is non-polar. Thus shape-dependent local-field effects will be small and we will neglect them.

The approach taken here is to account for the zeroth-order effect of particle size upon light scattering: We assume that there is no coupling between nonpolar phonons in different crystallites and that the scattering from each crystallite is added independently. However, within each crystallite we assume that the vibrational excitations of the small crystals are similar to those of the infinite crystal. The light scattering cross section is given by<sup>30</sup>

$$\frac{d^2\sigma}{d\Omega d\omega_s} = \left(\frac{\omega_s}{c}\right)^4 \left(\frac{V^2 \omega_s}{2\pi\omega_i}\right) S(\vec{k}, \omega), \quad (3)$$

where  $V$  is the illuminated volume,  $\omega_s$  and  $\omega_i$  are the frequencies of the incident and scattered photons,  $\omega = \omega_s - \omega_i$  is the frequency difference,

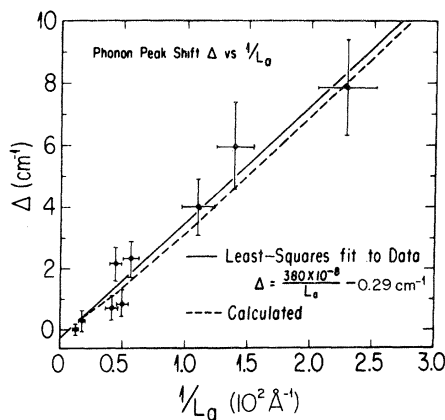


FIG. 6. The dependence of the peak position of the high-frequency  $E_{2g}$  mode versus  $1/L_a$ . The solid line is a least-squares fit to the data with the indicated values. The dashed lines represent the calculated peak position using the model presented in Secs. III C and III D.

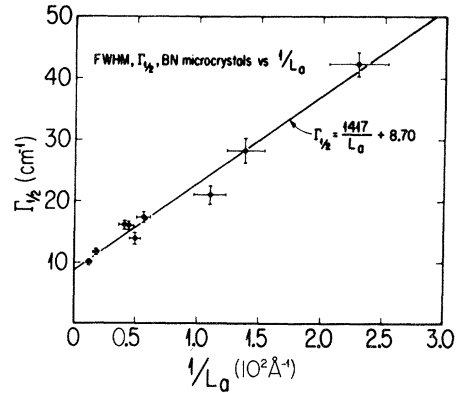


FIG. 7. The dependence of the peak width  $\Gamma_{1/2}$ , of the high-frequency  $E_{2g}$  mode versus  $1/L_a$ . The solid line is a least-squares fit to the data with the indicated values.

and  $\vec{k}$  is the wave-vector transfer

$$\vec{k} = \vec{k}_i - \vec{k}_s. \quad (4)$$

The dynamic structure factor  $S(\vec{k}, \omega)$  is the Fourier transform of the correlation function of the fluctuations in the polarizability  $\delta\chi_{ij}(\vec{r}, t)$

$$S(\vec{k}, \omega) = V^{-2} \text{Im} \int d\vec{r} \int d\vec{r}' \int dt \langle \delta\chi^*(\vec{r}, t) \delta\chi(\vec{r}', 0) \rangle \times \exp[-i\vec{k} \cdot (\vec{r} - \vec{r}') - i\omega t]. \quad (5)$$

The polarizability fluctuations are related to phonon displacements to linear order by

$$\delta\chi_{ij}(\vec{r}, t) = A_{ij} u(\vec{r}, t), \quad (6)$$

so that  $S(\vec{k}, \omega)$  is proportional to a phonon-displacement correlation function. Our assumption is that the coefficients  $A_{ij}$  and the displacement correlation function within each crystallite are the same as in a perfect crystal. In that case phonons of different  $\vec{q}$  are uncorrelated and

$$\langle u^*(\vec{r}, t) u(\vec{r}', 0) \rangle = V^{-1} \sum_{\vec{q}} \langle u^*(\vec{q}) u(\vec{q}) \rangle \times \exp[i\vec{q} \cdot (\vec{r} - \vec{r}') + i\omega_0(\vec{q})t], \quad (7)$$

where  $\omega_0(\vec{q})$  are the intrinsic phonon dispersion curves. Because the correlation function in Eq. (7) depends only on the difference  $\vec{r} - \vec{r}'$ , the integrals in the structure factor  $S(\vec{k}, \omega)$  can be factorized and  $S(\vec{k}, \omega)$  can be written

$$S(\vec{k}, \omega) = \left(\frac{N}{V^2}\right) V^{-1} \sum_{\vec{q}} |A_{ij}(\vec{q})|^2 \delta(\omega - \omega_0(\vec{q})) \times \langle u^*(\vec{q}) u(\vec{q}) \rangle |F(\vec{k} - \vec{q})|^2. \quad (8)$$

Here  $N$  is the number of crystallites in the volume  $V$  and  $F$  is the integral over  $\vec{r}$  or  $\vec{r}'$  restricted to a single crystallite. Then

$$F(\vec{k} - \vec{q}) = \int d\vec{r} \exp[i(\vec{k} - \vec{q}) \cdot \vec{r}]. \quad (9)$$

If we assume the crystallites are orthorhombic in shape with dimensions  $L_x$ ,  $L_y$ , and  $L_z$ , then  $F$  has the familiar Scherrer form<sup>27,31</sup>

$$F(\vec{k} - \vec{q}) = \prod_{i=x,y,z} 2 \sin[(q_i - k_i)L_i/2]/(q_i - k_i). \quad (10)$$

Finally, we note that the displacement correlation function in the infinite crystal can be expressed in terms of the boson occupation numbers  $n(\omega)$ .<sup>32</sup> Collecting all coefficients into a single effective "matrix element"  $C(q, \omega)$ , we can write the dynamical structure factor for Stokes scattering as

$$S(\vec{k}, \omega) = \frac{N}{V^2} \left( \frac{n(\omega) + 1}{\omega} \right) V^{-1} \sum_{\vec{q}} C(\vec{q}, \omega) |F(\vec{q} - \vec{k})|^2 \times \delta(\omega - \omega_0(\vec{q})). \quad (11)$$

If a lifetime for the phonons is included as a Lorentzian broadening  $\Gamma_{1/2}$ , then Eq. (11) is modified to read

$$S(\vec{k}, \omega) = \frac{N}{V^2} \left( \frac{n(\omega) + 1}{\omega} \right) V^{-1} \times \sum_{\vec{q}} \alpha(\vec{q}, \omega_0(\vec{q})) |F(\vec{q} - \vec{k})|^2 (\Gamma_{1/2}/4\pi) \times \{ [\omega - \omega_0(\vec{q})]^2 + (\Gamma_{1/2}^2/4) \}^{-1}. \quad (12)$$

For finite crystallites the function  $|F(\vec{q} - \vec{k})|^2$  represents the wave-vector "uncertainty" in the phonons involved in the light scattering event. We examine this function with respect to the usual uncertainty relation. The first minimum in  $F^2$  occurs at  $k_i - q_i = 2\pi/L_i$  ( $i=x, y, z$ ). Thus for scattering from small crystals light will couple to excitations with wave vectors in the range of  $k_i \pm 2\pi/L_i$ . This means that a larger region of the Brillouin zone is sampled. If the phonon dispersion curves vary significantly in the region near  $\vec{q} \approx 0$ , spectral features could shift or broaden or new features could occur. However, if the phonon dispersion curves are flat then relatively little spectral change will occur.

It is interesting to examine the form of Eq. (12) in the limits of large and small structures. For a very large crystal  $F$  becomes a delta function and the spectrum becomes a sum of weighted Lorentzians, which is typical of large crystals. In the

small structure limit we can consider amorphous materials. It is not unreasonable to write the vibrational excitations of an amorphous material in terms of a Fourier series based on the vibrations of the crystalline counterpart, since local atomic structure is often preserved in the amorphous form.<sup>33</sup> The spatial integration would then be limited by the size of the local atomic structures, and  $F(\vec{k} - \vec{q})$  would be so broad as to allow scattering from all excitations. The dynamic structure factor becomes

$$S(\vec{k}, \omega) = \frac{N}{V\omega} [n(\omega) + 1] \sum_{\omega_0} C(\omega_0) (\Gamma_{1/2}/4\pi) \times [(\omega - \omega_0)^2 + (\Gamma_{1/2}/2)^2]^{-1}, \quad (13)$$

where the  $\omega_0$  are now the vibrational eigenfrequencies of the amorphous material. Expressions similar to this have been proposed to describe light scattering from amorphous materials.<sup>34</sup> We note that if  $C(\omega_0)$  is a constant, then the sum over  $\omega_0$  yields a Lorentzian-broadened density of states. Several studies have suggested that the Raman spectra of some amorphous materials may be related to the broadened crystalline density of states.<sup>33</sup> Recently, however, it has been shown that the coupling constant  $C$  can not be considered as a constant independent of frequency. For instance, at very low frequency,  $C \propto \omega^2$  (Refs. 35 and 36) and striking variations of  $C$  exist in certain cases where rather sharp band edges can be shown to exist in amorphous materials.<sup>37</sup>

#### D. Application to BN results

In this section the changes in the Raman spectra of BN microcrystallites are analyzed in terms of the results of the preceding section. To apply Eq. (12) it is necessary to have a reasonable description of the phonon dispersion relations. There have been to our knowledge no neutron scattering measurements or accurate calculations of the phonon dispersion curves of BN. However, the similar material, graphite, has been the subject of several such studies, and we can use these results with a reasonable degree of confidence.<sup>10,38-42</sup> The results of these studies indicate that there is little dispersion of the high-frequency  $E_{2g}$  mode for  $\vec{q}$  along the  $c$  axis. In addition, for  $q_x$  and  $q_y$  the dispersion relations are almost identical near the zone center. Thus the phonon dispersion relations exhibit approximate axial symmetry, and  $L_a$  is the important crystal-size parameter. According to the preceding section the wave-vector uncertainty is

$\approx 2\pi/L_a$ , which for the samples studied here would vary from  $\sim 6 \times 10^5$  to  $\sim 20 \times 10^5 \text{ cm}^{-1}$ . Two important quantities to contrast with this range are the scattering wave vector in the sample and the zone-boundary wave vector. For the scattering configuration used the wave vector transferred is  $\sim 3 \times 10^5 \text{ cm}^{-1}$  and a zone-boundary wave vector is  $\sim 300 \times 10^5 \text{ cm}^{-1}$ . Thus the wave-vector transfer is small compared to the uncertainty region in which  $\sim 10\%$  of the Brillouin zone is sampled.

The calculations of the phonon dispersion of the  $E_{2g}$  mode for graphite show that the mode splits for  $q_x$  or  $q_y$  increasing from  $\Gamma$ . In the region of interest the upper branch exhibits an almost linear increase with  $q_x$  or  $q_y$ , while the lower branch exhibits a larger negative dispersion.<sup>10,38</sup> This large negative dispersion of the lower mode means its contribution will be spread over a much larger frequency range. Hence there will be a small, if not negligible contribution, to the scattering from the lower branch. Thus to approximate the phonon dispersion of BN the slope ( $A$ ) of the phonon dispersion curve of the high-frequency branch of the  $E_{2g}$  mode was obtained from the corresponding value reported by Nicklow *et al.* for graphite.<sup>38</sup> We then used the functional form

$$\omega_0(q) = \{[(Aq_x)^2 + 0.2^2]^{1/2} + 1366\}, \quad (14)$$

in units of  $\text{cm}^{-1}$ , for the relevant dispersion curve of BN. The addition of the  $0.2^2$  term assured that the slope at  $\vec{q}=0$  was 0. The value of  $A$  used was  $5.63 \times 10^{-7} \text{ cm}^2$ .

We approximated the function  $F$  by a Gaussian centered at  $q=0$  (i.e., the scattering wave vector  $\vec{k}$  is approximately 0) with a HWHM of  $2\pi/L_a$ . We suggest that a Gaussian-functional form is more appropriate than  $[\sin^2(qL/2)]/q$  because there is most likely a distribution of particle sizes in the samples we used. We have not attempted to explicitly determine the particle-size distribution from our data. Such a determination could, in principle, be made using electron microscopy.

Initially we evaluated Eq. (12) using the above restrictions and assumed a constant lifetime characterized by the narrowest measured width ( $8.5 \text{ cm}^{-1}$ ). We found that the calculated peak frequency shifted to higher values (consistent with the experiment), but the widths were much narrower than those measured. It is likely, however, that the vibrational excitation lifetimes are strongly influenced by surface and boundary scattering effects. If this is the case, then the surface-to-volume ratio is the important parameter. Thus we assumed that the Lorentzian linewidth was dependent on crystal domain size and was given by

$$\Gamma_{1/2} = A + B/L_a. \quad (15)$$

The parameters  $A$  and  $B$  were determined from the least-squares fit to the data shown in Fig. 7. For each observed value  $L_a$ , the predicted Raman spectrum was evaluated using this crystal-size dependence of  $\Gamma_{1/2}$ , and a very good fit to the data was obtained. This fit was only slightly improved by varying  $A$  and  $B$ . Two examples of the fits are shown in Fig. 8. In addition, plotted in Fig. 6 is the calculated variation of the peak position on  $1/L_a$ . As is seen, an excellent agreement with observation was obtained. We should note that all effects due to surface and interface bonding have been ignored, but the good agreement demonstrated here suggests that these effects may be small.

#### IV. CONCLUDING REMARKS

In this study it was found that crystal size affects the Raman spectra in an indirect way. To achieve a shift in spectral features, significant dispersion must exist in the phonon frequencies. This is to be contrasted with x-ray diffraction, where the angular width of diffraction peaks can be directly related to the crystallite size.<sup>27</sup> For the case of BN the Raman band associated with the nonpolar intralayer mode shifts to higher frequency with decreasing crystal size. This shift is basically a manifestation of the unusual dispersion curves which BN is expected to have, i.e., the phonon frequency of the highest branch is not a maximum at the  $\Gamma$  point. For most crystalline solids the reverse is true, and one would expect a decrease in the Raman shift of the highest-frequency nonpolar mode with decreasing crystallite size. One example of recent interest is the interpretation of the Raman spectrum of

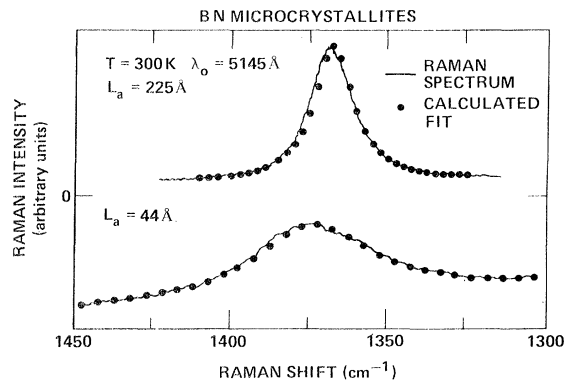


FIG. 8. Fits to two of the spectra using the model presented in Secs. III C and III D.

polycrystalline or laser-crystallized Si.<sup>13,14</sup> The Raman spectrum of these materials shows a downshift of the strongest line for the materials associated with the smallest crystalline domain sizes. The phonon dispersion curves of crystalline Si are well known, and the Raman-active phonon is at the maximum frequency. The wave-vector effects described here would predict the downshifting of the Raman-active mode, which is consistent with the observation.

It is now interesting to reflect on the first- and second-order Raman results of microcrystalline graphite.<sup>8,10,12</sup> In the first-order spectrum the peak associated with the high-frequency intralayer  $E_{2g}$  mode broadens and shifts to higher frequency, as in BN. However, this is not the most striking effect. Two new features are observed at 1357 and 1621  $\text{cm}^{-1}$ . These features seem to correspond to peaks in the density of states.<sup>10</sup> It seems to us that the absence of these features in BN is an indication that unusual matrix element effects must enhance these features in graphite. The second-order spectrum of graphite also shows interesting changes which were attributed to breakdown of the wave-vector selection rules.<sup>10,11</sup> We were, however, unable to observe the second-order spectrum of BN.

Unfortunately there are relatively few other materials which can be prepared as powders of three-dimensional crystals with sufficiently small sizes to carry out a study such as the one reported here. However, the matrix isolation technique which was used so effectively by Martin *et al.*<sup>43</sup> to study the ir absorption of small uniform ionic

crystals should also be useful for Raman studies of both ionic and covalent materials. In addition, recent experimental advances have made possible the observation of intense Raman signals from very thin films.<sup>44</sup> Such films might be used to systematically study finite-size effects in one dimension for both polar and nonpolar modes. In particular it should be straightforward to distinguish the bulk modes from the surface modes by varying the film thickness.

Perhaps the main difficulty in dealing with studies of very small ( $L \ll \lambda$ ) particles is in adequately characterizing the crystallite size and shape. Several authors have suggested that for such particles the polar optical properties are shape and size independent. This is true only if one ignores the more subtle effects we have addressed in this paper.

#### ACKNOWLEDGMENTS

We are grateful to D. Dennison for technical assistance with sample preparation and to A. W. Moore for providing the compression-annealed highly oriented BN used in part of this work. This work was initiated while two of us (R.J.N. and S.A.S.) were at the University of Chicago and was supported in part by USDOE Grant No. DOEY-76-S-02-2126. One of us (S.A.S.) acknowledges continuing support for this work from the NSF under Grant No. DMR-78-11568 and is grateful to Xerox Palo Alto Research Centers for their hospitality during the preparation of this manuscript.

- 
- <sup>1</sup>R. Ruppin and R. Englman, *Rep. Prog. Phys.* **33**, 149 (1970).
- <sup>2</sup>R. Ruppin and R. Englman, in *Light Scattering Spectra of Solids*, edited by G. B. Wright, (Springer, New York, 1969), p. 157.
- <sup>3</sup>I. R. Nair and C. T. Walker, *Phys. Rev. B* **5**, 4101 (1972).
- <sup>4</sup>J. F. Scott and T. C. Damen, *Opt. Commun.* **5**, 410 (1972).
- <sup>5</sup>R. G. Schlecht and H. K. Böckelmann, *Phys. Rev. Lett.* **31**, 930 (1973).
- <sup>6</sup>T. P. Martin and L. Genzel, *Phys. Rev. B* **8**, 1630 (1973).
- <sup>7</sup>M. Hass and H. B. Rosenstock, *Appl. Opt.* **6**, 2079 (1967).
- <sup>8</sup>F. Tuinstra and J. L. Koenig, *J. Chem. Phys.* **53**, 1126 (1970).
- <sup>9</sup>R. J. Nemanich, G. Lucovsky, and S. A. Solin, *Mater. Sci. Eng.* **31**, 157 (1977).
- <sup>10</sup>R. J. Nemanich and S. A. Solin, *Phys. Rev. B* **20**, 392 (1979).
- <sup>11</sup>R. B. Wright, R. Varma, and D. M. Gruen, *J. Nucl. Mater.* **63**, 415 (1976).
- <sup>12</sup>R. Tsu, J. Gonzalez H., and I. Hernandez C., *Solid State Commun.* **27**, 507 (1978).
- <sup>13</sup>F. Morhange, G. Kanellis, M. Balkanski, J. F. Peray, J. Icote, and M. Croset, in *Laser-Solid Interactions and Laser Processing—1978 (Materials Research Society, Boston)*, edited by S. D. Ferris, H. J. Leamy, and J. M. Poate (AIP, New York, 1978), 429.
- <sup>14</sup>S. Veprek, Z. Iqbal, H. R. Oswald, and A. P. Webb, *J. Phys. C* **14**, 295 (1981).
- <sup>15</sup>G. Kanellis, J. F. Morhange, and M. Balkanski, *Phys. Rev. B* **21**, 1543 (1980).
- <sup>16</sup>F. P. Bundy and R. H. Wentorf, Jr., *J. Chem. Phys.* **38**, 1144 (1963).
- <sup>17</sup>R. S. Pease, *Acta Crystallogr.* **5**, 356 (1952).
- <sup>18</sup>R. G. Wyckoff, *Crystal Structures* (Interscience, New York, 1963), Vol. 1, p. 184.
- <sup>19</sup>J. Thomas, Jr., N. E. Weston, and T. E. O'Connor, *J. Am. Chem. Soc.* **84**, 4619 (1963).
- <sup>20</sup>R. Geick, C. H. Perry, and G. Rupprecht, *Phys. Rev.* **146**, 543 (1966).
- <sup>21</sup>R. J. Nemanich and S. A. Solin, *Bull. Am. Phys. Soc.*

- 20, 429 (1975).
- <sup>22</sup>T. Kuzuba, K. Era, T. Iahii, and T. Sato, *Solid State Commun.* 25, 863 (1978).
- <sup>23</sup>T. Kuzuba, Y. Sato, S. Yamaoka, and K. Era, *Phys. Rev. B* 18, 4440 (1978).
- <sup>24</sup>T. E. O'Connor, *J. Am. Chem. Soc.* 84, 1753 (1962).
- <sup>25</sup>T. E. O'Connor, U. S. Patent No. 3241919, 1966.
- <sup>26</sup>A. W. Moore, *Nature (London)* 221, 1133 (1969).
- <sup>27</sup>B. E. Warren, *X-ray Diffraction* (Addison-Wesley, Reading, Mass., 1969), p. 253.
- <sup>28</sup>W. Baronian, *Mater. Res. Bull.* 7, 119 (1972).
- <sup>29</sup>R. J. Nemanich, G. Lucovsky, and S. A. Solin, in *Lattice Dynamics*, edited by M. Balkanski (Flammarion, Paris, 1975), p. 619.
- <sup>30</sup>A. Pinczuk and E. Burstein, in *Topics in Applied Physics*, edited by M. Cardona (Springer, New York, 1975), Vol. 8, p. 23.
- <sup>31</sup>See, for example, A. Messiah, *Quantum Mechanics* (Wiley, New York, 1961), Vol. 1, p. 131.
- <sup>32</sup>See, for example, Marshall and Lovesey, *Theory of Thermal Neutron Scattering* (Clarendon, Oxford, 1971), p. 58.
- <sup>33</sup>M. H. Brodsky, in *Topics in Applied Physics*, edited by M. Cardona (Springer, New York, 1975), Vol. 8, p. 203.
- <sup>34</sup>R. Shuker and R. Gamon, *Phys. Rev. Lett.* 25, 222 (1970).
- <sup>35</sup>J. S. Lannin, *Solid State Commun.* 12, 947 (1973).
- <sup>36</sup>R. J. Nemanich, *Phys. Rev. B* 16, 1655 (1977).
- <sup>37</sup>F. L. Galeener, *Phys. Rev. B* 19, 4292 (1979); Richard M. Martin and F. L. Galeener, *Phys. Rev. B* 23, 3071 (1981).
- <sup>38</sup>R. Nicklow, N. Wakabayashi, and H. G. Smith, *Phys. Rev. B* 5, 4951 (1972).
- <sup>39</sup>A. A. Ahmadiéh and H. A. Rafizadeh, *Phys. Rev. B* 7, 4527 (1973).
- <sup>40</sup>K. K. Mani and R. Ramani, *Phys. Status Solidi B* 61, 659 (1974).
- <sup>41</sup>A. P. P. Nicholson and D. J. Bacon, *J. Phys. C* 10, 2295 (1977).
- <sup>42</sup>R. J. Nemanich and S. A. Solin, *Solid State Commun.* 23, 417 (1977).
- <sup>43</sup>T. P. Martin, private communication.
- <sup>44</sup>G. A. N. Connell, R. J. Nemanich, and C. C. Tsai, *Appl. Phys. Lett.* 36, 31 (1980).